



Contents lists available at ScienceDirect



Catalysis Today

journal homepage: www.elsevier.com/locate/cattod

Spectroscopic investigation of sulfur-resistant Pt/K₂O/ZrO₂/TiO₂/Al₂O₃ NSR/LNT catalysts

Z. Say, M. Tohumeken, E. Ozensoy*

Department of Chemistry, Bilkent University, 06800 Ankara, Turkey

ARTICLE INFO

Article history:

Received 6 October 2015

Received in revised form

25 November 2015

Accepted 4 December 2015

Available online xxx

Keywords:

NSR/LNT

DeNO_x Al₂O₃/ZrO₂/TiO₂

FTIR

TPD

ABSTRACT

An alternative ternary support oxide material and its K₂O and Pt functionalized counterparts in the form of Pt/K₂O/Al₂O₃/ZrO₂/TiO₂ with different K₂O loadings were synthesized. Structural and morphological properties of the catalysts were characterized via XRD and BET techniques in comparison to a conventional Pt/20Ba/Al benchmark NSR/LNT catalyst. Comprehensive *in-situ* FTIR and TPD analysis revealed that increasing the K₂O loading in the Pt/K₂O/AZT system leads to an increase in NO_x Storage Capacity (NSC) at the expense of the formation of bulk-like sulfates requiring higher temperature for complete sulfur elimination with H₂(g). Observed delicate trade-off between NSC and sulfur poisoning tendencies of the currently investigated family of AZT-based NSR/LNT catalysts implies that Pt/5.4K₂O/AZT is a promising catalyst revealing comparable NSC within the temperature range of 473–673 K to that of the conventional Pt/20Ba/Al benchmark catalyst, while exhibiting superior sulfur tolerance and regeneration characteristics.

© 2016 Elsevier B.V. All rights reserved.

1. Introduction

NO_x emitted from mobile sources have serious destructive effects on the atmosphere, global ecosystem and especially on the human health. About one half of the total NO_x emissions results from mobile sources [1]. While the very first regulations for diesel engine emissions were primarily focusing on particle emissions, other hazardous pollutants such as CO, SO₂, NO_x and unburned hydrocarbons from mobile sources are currently being regulated with increasingly stringent limitations. This leads to a constant pressure on the global automotive industry to develop novel and innovative aftertreatment technologies that can satisfy the continuously evolving environmental legislations and to lower the exhaust emission levels [2–4]. Recently, it was reported that NO_x emissions of some of the currently existing diesel-engine passenger cars equipped with modern DeNO_x aftertreatment systems on the highway were up to 20–35 times higher than that of the allowed emission limits [5]. Furthermore, a very recent study published by the European Environment Agency (EEA) [6] reported that without

any exception, each European Union (EU) member state violates at least one or more of the existing annual emission limitations associated with NO_x, SO_x, NH₃ and non-methane volatile organic compounds (NMVOC). Among these EU member states, particularly Germany, Austria and Ireland were found to fail meeting annual European NO_x emission standards in 2014. These striking examples clearly call for the design and development of more efficient, more stable and more affordable heterogeneous catalytic architectures that can be used in modern DeNO_x aftertreatment technologies.

For lean-burn engines, a promising aftertreatment method for the catalytic NO_x reduction is the so called NO_x storage/reduction (NSR)/Lean NO_x Trap (LNT) technology [7,8]. A typical NSR/LNT catalyst is comprised of basic oxides (e.g. BaO, K₂O), redox sites (e.g. Pt, Pd and/or Rh) and a high surface area support material (e.g. γ-Al₂O₃) [2,3,9].

The conventional NSR/LNT catalyst, Pt/BaO/γ-Al₂O₃, exhibits efficient NO_x conversion and storage performance within the operational temperature window of the diesel emission tail pipe (*i.e.* 473–673 K) [10–18]. However, recent engine applications such as the fuel-efficient gasoline direct injection (GDI) engines require catalytic aftertreatment solutions which should be able to operate at temperatures above 400 °C, where the conventional NSR/LNT catalysts cannot function effectively [19]. Toyota Motor Company

* Corresponding author.

E-mail address: ozensoy@fen.bilkent.edu.tr (E. Ozensoy).

reported that K₂O and BaO are two of the most promising NO_x storage components to be used in NSR/LNT catalysts [20]. Among these two different types of basic metal oxides, the use of K₂O attracted particular interest due to its superior NO_x storage capacity (NSC) at elevated temperatures [21]. Other noteworthy advantages of K₂O domains are associated to their stronger basicity and the lack of unfavorable solid-state interactions between K₂O and the γ -Al₂O₃ support material, unlike that of BaO which may lead to the formation of undesired BaAl₂O₄ at high temperatures [22]. Luo et al. investigated the effect of K₂O loading (within 2–20 wt. %) on the NSC of the Pt/K₂O/ γ -Al₂O₃ system. It was found out that the catalyst formulation containing 10 wt. % K₂O resulted in the highest NSC values within a wide temperature window of 523–823 K [22].

In addition to the promising NSC of K₂O-functionalized materials in high temperature DeNO_x applications, sulfur-poisoning tolerances as well as the sulfur regeneration characteristics of such systems should be also taken into consideration. It is known that K₂O domains dispersed on a γ -Al₂O₃ support material are highly prone to sulfur poisoning, experiencing rapid and rather irreversible catalytic deactivation. A class of novel Al/Ti/Zr mixed oxides has emerged in recent years with enhanced surface and structural properties as support for K₂O-based NSR/LNT catalysts [23–25]. In recent studies, ZrO₂/TiO₂, TiO₂/Al₂O₃ and Al₂O₃/ZrO₂/TiO₂-supported NSR/LNT catalysts can reveal superior sulfur regeneration and NO_x recovery performances as compared to that of γ -Al₂O₃-based systems (*i.e.* Pt/BaO/Al₂O₃ vs. Pt/K₂O/Al₂O₃) [26,27]. Takashi et al. reported that a ZrO₂:TiO₂ support material with a mass ratio of 70:30 (which also revealed the highest SSA among the investigated materials therein) exhibited the best performance in terms of sulfur resistance, thermal durability and NO_x abatement [28]. Their studies which also included Pt/Rh/Ba/K/AZT catalyst with nano-composite ternary oxide Al₂O₃/ZrO₂/TiO₂-support showed excellent NO_x storage capacity (NSC) compared to that of γ -Al₂O₃/ZrO₂/TiO₂-support, where γ -Al₂O₃ was physically mixed with ZrO₂/TiO₂ [29,30]. In addition, Zou et al. [27] performed a detailed analysis on the effect of Al₂O₃ doping into the ZrO₂/TiO₂ matrix, suggesting that the Al:(Ti + Zr) atomic ratio of 3:1 exhibited the highest NSC for fresh and sulfur-regenerated catalyst. In a more recent work, Zou et al. studied the effect of K loading on the NSC and sulfur regeneration performance of Pt/K/Al₂O₃/ZrO₂/TiO₂ catalyst under realistic flow conditions [31].

However, these aforementioned comprehensive studies included a limited number of spectroscopic investigations on the interactions between SO_x species and the corresponding catalyst surfaces. Thus, in the current work, we focus on the molecular level investigation of the fundamental interactions that take place between SO_x species and K-based novel NSR/LNT catalyst surfaces in a qualitative and a semi-quantitative manner. Along these lines, we investigate the SO_x adsorption/uptake as well as the SO_x reduction/regeneration/release properties of Al₂O₃/ZrO₂/TiO₂ (AZT) supported Pt/K/AZT catalysts in comparison to a benchmark NSR/LNT catalyst (*i.e.* Pt/BaO/Al₂O₃) by utilizing *in-situ* spectroscopic techniques. Generation of S-containing surface functional groups, their thermal evolution, reduction and releases a function of temperature and K₂O loading are systematically monitored by means of *in-situ* Fourier Transform Infrared Spectroscopy (*in-situ* FTIR) and Temperature Programmed Desorption (TPD). Moreover, structural and morphological properties of the synthesized materials are also analyzed via X-ray Diffraction (XRD) and Brunauer, Emmett and Teller (BET) surface area analysis techniques. Current results provide valuable molecular level insight regarding the interaction of SO_x species with K-based NSR/LNT catalysts supported on novel AZT mixed oxide surfaces and the delicate trade-off between the NSC and sulfur poisoning phenomena.

2. Experimental

2.1. Material synthesis

2.1.1. Synthesis of Pt/Al₂O₃/ZrO₂/TiO₂

Al₂O₃/ZrO₂/TiO₂ (AZT) support material was synthesized as described in one of our former publications where the relative composition of the ternary oxide system (*i.e.* Al₂O₃/ZrO₂/TiO₂) by mass was 50:35:15 [25]. 1 wt. % platinum-incorporated ternary oxide materials were synthesized by incipient wetness impregnation method using a solution of Pt(NH₃)₂(NO₂)₂ (Aldrich, diamminedinitriplatinum(II), 3.4 wt.% solution in dilute NH₃(aq)). Prior to the Pt addition, Al₂O₃/ZrO₂/TiO₂ was initially calcined in air at 973 K for 150 min in order to remove the organic functionalities in the precursor. After the Pt-incorporation, Pt/AZT material was subsequently calcined in air at 973 K for 150 min in order to remove nitrite/nitrate originating from the Pt precursor and to structurally stabilize the catalyst surface.

2.1.2. Synthesis of Pt/K₂O/Al₂O₃/ZrO₂/TiO₂

K₂O-based catalysts were also prepared *via* wetness impregnation. Pt/K₂O/Al₂O₃/ZrO₂/TiO₂ catalysts with 2.7, 5.4 and 10.0 wt. % K₂O loading (*i.e.* Pt/2.7K₂O/Al₂O₃/ZrO₂/TiO₂, Pt/5.4K₂O/Al₂O₃/ZrO₂/TiO₂ and Pt/10K₂O/Al₂O₃/ZrO₂/TiO₂; respectively) were prepared *via* impregnation of Al₂O₃/ZrO₂/TiO₂ support (initially calcined at 973 K for 150 min) with an aqueous solution of potassium nitrate (KNO₃·6H₂O, >99.0 %, Fluka, France) followed by calcination at 873 K for 150 min in order to thermally remove the nitrate content present in the precursors. Finally, K₂O/Al₂O₃/ZrO₂/TiO₂ structure was impregnated with the Pt(NH₃)₂(NO₂)₂ precursor and calcined at 973 K for 150 min under ambient conditions in order to attain 1 wt. % nominal precious metal loading. Throughout the current text, synthesized Pt/K₂O/Al₂O₃/ZrO₂/TiO₂ catalysts with 2.7, 5.4 and 10.0 wt. % K₂O and 1 wt. % Pt loadings will be abbreviated as Pt/2.7K/AZT, Pt/5.4K/AZT and Pt/10K/AZT, respectively.

2.1.3. Synthesis of Pt/BaO/ γ -Al₂O₃

For the synthesis of the Pt/20BaO/Al benchmark catalyst, γ -Al₂O₃ support material (SASOL Puralox, 210 m²/g) was impregnated with an aqueous solution of barium nitrate (Ba(NO₃)₂, ACS Reagent, ≥ 99%, Riedel-de Häen, Germany) which was followed by calcination at 873 K in air for 150 min. Finally, 20BaO/Al₂O₃ was impregnated with the Pt(NH₃)₂(NO₂)₂ precursor (Aldrich, diamminedinitriplatinum(II), 3.4 wt.% solution in dilute NH₃(aq)) to obtain 1 wt. % nominal precious metal loading, followed by calcination at 973 K for 150 min. This catalyst will be abbreviated as Pt/20Ba/Al throughout the current text.

2.2. Experimental setup

Comprehensive description of the custom-made batch-mode *in-situ* FTIR and TPD spectroscopic setup used in the current measurements can be found elsewhere [10,14,25,32]. Briefly, an FTIR spectrometer (Bruker Tensor 27) and a quadrupole mass spectrometer (QMS, Stanford Research Systems, RGA 200) were simultaneously connected to a batch-type spectroscopic reactor. FTIR experiments were performed in transmission mode. TPD profiles were obtained under vacuum by using a computer-controlled linear temperature ramp of 12 K/min with a maximum sample temperature of 1173 K.

2.3. Experimental procedures

2.3.1. Monitoring SO_x adsorption via in-situ FTIR

Sulfur adsorption/poisoning characteristics of each material was investigated by exposing the catalyst surfaces to a 2.0 Torr $\text{SO}_2 + \text{O}_2$ gas mixture ($\text{SO}_2:\text{O}_2 = 1:10$, v/v) at 323 K (SO_2 purity >99%, Air Products; O_2 purity > 99.999%, Linde GmbH). After the introduction of SO_x mixture at 323 K, samples were annealed to 373, 473, 573 and 673 K for 5 min in the presence of the SO_x mixture. FTIR spectra of these sulfated surfaces were acquired after cooling to 323 K in the presence of the gas mixture and subsequent evacuation to $< 10^{-3}$ Torr. It should be noted that the effective concentration of SO_2 used in the current poisoning experiments corresponds to ca. 263 ppm (in a balance carrier gas under flow conditions), which translates into extremely severe poisoning conditions considering the typical sulfur content (15 ppm) of Ultra Low Sulfur Diesel (ULSD) fuel. Thus, the current poisoning experiments can be assessed as accelerated and extreme sulfur poisoning experiments, where the novel K-AZT based catalysts were exposed to particularly challenging conditions, where they can demonstrate their ultimate sulfur-regeneration capabilities.

2.3.2. Monitoring SO_x desorption via in-situ FTIR

Prior to SO_x desorption experiments, materials were sulfated as described above by collecting a series of *in-situ* FTIR spectra in the presence of the SO_x mixture as a function of temperature until 673 K. After the saturation of the surfaces with sulfur at 673 K, the reactor was evacuated to a pressure of $< 10^{-2}$ Torr, followed by the introduction of 15.0 Torr of $\text{H}_2(\text{g})$ (H_2 purity > 99.999%, Linde GmbH) at 323 K. Next, poisoned catalysts were annealed under hydrogen atmosphere at 473, 673, 773, 873 and 973 K for 5 min. *In-situ* FTIR spectra were obtained after each H_2 exposure and by cooling the sample to 323 K in the presence of H_2 .

2.3.3. SO_x desorption via TPD

Before the SO_x -TPD experiments, material surfaces were initially exposed to a 2.0 Torr $\text{SO}_2 + \text{O}_2$ gas mixture ($\text{SO}_2:\text{O}_2 = 1:10$) at 673 K for 30 min. Then the IR spectroscopic reactor was evacuated to a pressure lower than 10^{-3} Torr followed by heating under vacuum to 1173 K with a linear heating rate of 12 K/min. In the TPD experiments, $m/z = 32$ (corresponding to $\text{O}_2(\text{g})$ desorption and $\text{S}(\text{g})$ formation due to the impact ionization-induced fragmentation of desorbed $\text{SO}_2(\text{g})$ species in QMS) and $m/z = 64$ (corresponding to $\text{SO}_2(\text{g})$ desorption) channels were monitored via QMS.

3. Results and discussion

3.1. Material characterization

3.1.1. X-ray diffraction analysis (XRD)

Fig. 1 illustrates the XRD patterns of Pt/AZT, Pt/2.7K/AZT, Pt/5.4K/AZT, Pt/10K/AZT and Pt/20Ba/Al. Apart from the presence of structurally well-ordered metallic platinum (JCPDS 001-1190), Pt/AZT and Pt/K/AZT catalysts given in **Fig. 1** exhibit highly amorphous characteristics. On the other hand, material with 10.0 wt. % K_2O (i.e. Pt/10.0K/AZT) reveals additional poorly discernible diffraction signals at $2\theta = 30.48^\circ, 50.50^\circ, 60.91^\circ$ corresponding to tetragonal ZrO_2 (JCPDS 80-2155) together with some suppression of Pt diffraction features. XRD analysis of the benchmark Pt/20Ba/Al NSR/LNT catalyst reveals $\gamma\text{-Al}_2\text{O}_3$ (JCPDS 001-1303), BaAl_2O_4 (JCPDS 017-0306) and metallic Pt (JCPDS 001-1190) features. On the Pt/20Ba/Al catalyst, BaO domains interact with the $\gamma\text{-Al}_2\text{O}_3$ support at elevated temperatures yielding the formation of undesired BaAl_2O_4 phase as a result of thermal aging [2,3,33].

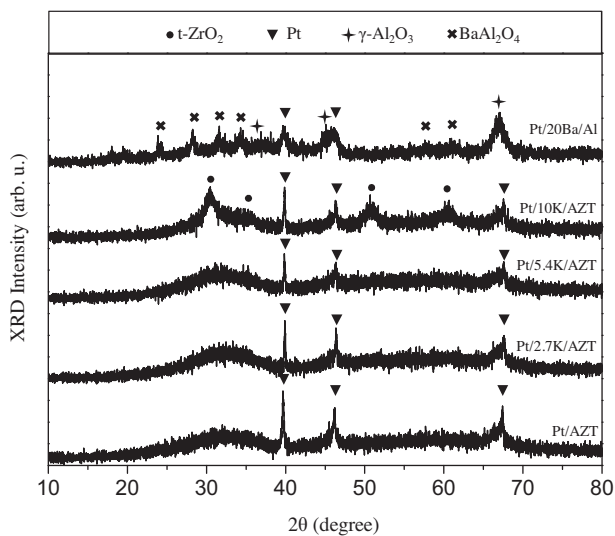


Fig. 1. XRD patterns corresponding to Pt/AZT, Pt/2.7K/AZT, Pt/5.4K/AZT, Pt/10K/AZT and Pt/20Ba/Al materials upon calcination at 973 K.

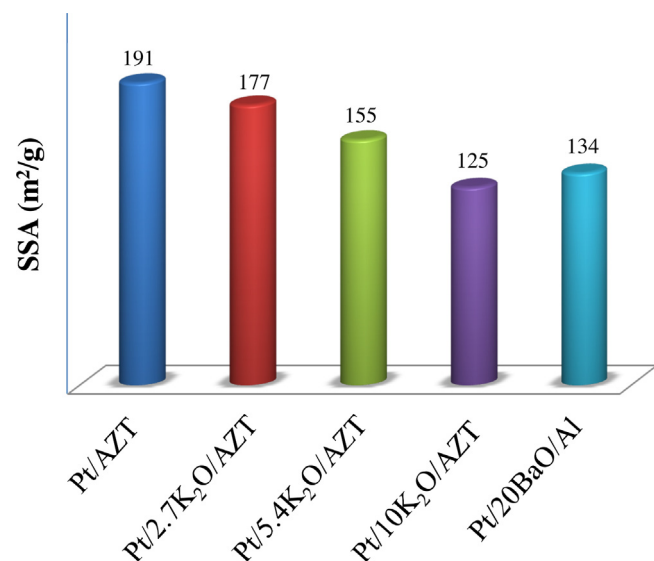


Fig. 2. BET specific surface area (SSA) values of the investigated materials.

3.1.2. BET specific surface area (SSA) measurements

Fig. 2 illustrates SSA values for Pt/AZT, Pt/2.7K/AZT, Pt/5.4K/AZT, Pt/10K/AZT and Pt/20Ba/Al. SSA values for Pt/AZT is slightly higher than 2.7 wt. % K_2O -modified counterpart (i.e. Pt/2.7K/AZT). However, increase in the K_2O loading from 2.7 wt. % to 5.4 and 10.0 wt. % monotonically decreases SSA values from 177 m^2/g to 155 and 125 m^2/g ; respectively. It should be noted that the SSA value of the catalyst with the highest K_2O loading was comparable to that of the benchmark Pt/20Ba/Al catalyst (134 m^2/g), while SSA values of all of the other catalysts were relatively higher.

3.2. SO_x Uptake/adsorption via in-situ FTIR spectroscopy

Fig. 3 represents temperature-dependent adsorbed SO_x species on Pt/AZT, Pt/2.7K/AZT, Pt/5.4K/AZT and Pt/10K/AZT material surfaces upon exposure to 2.0 Torr of $\text{SO}_2 + \text{O}_2$ gas mixture ($\text{SO}_2:\text{O}_2 = 1:10$). While the black-colored spectra in each panel correspond to the surface SO_x species generated within a temperature range of 323–573 K, the topmost red spectra correspond to sulfur poisoning at 673 K.

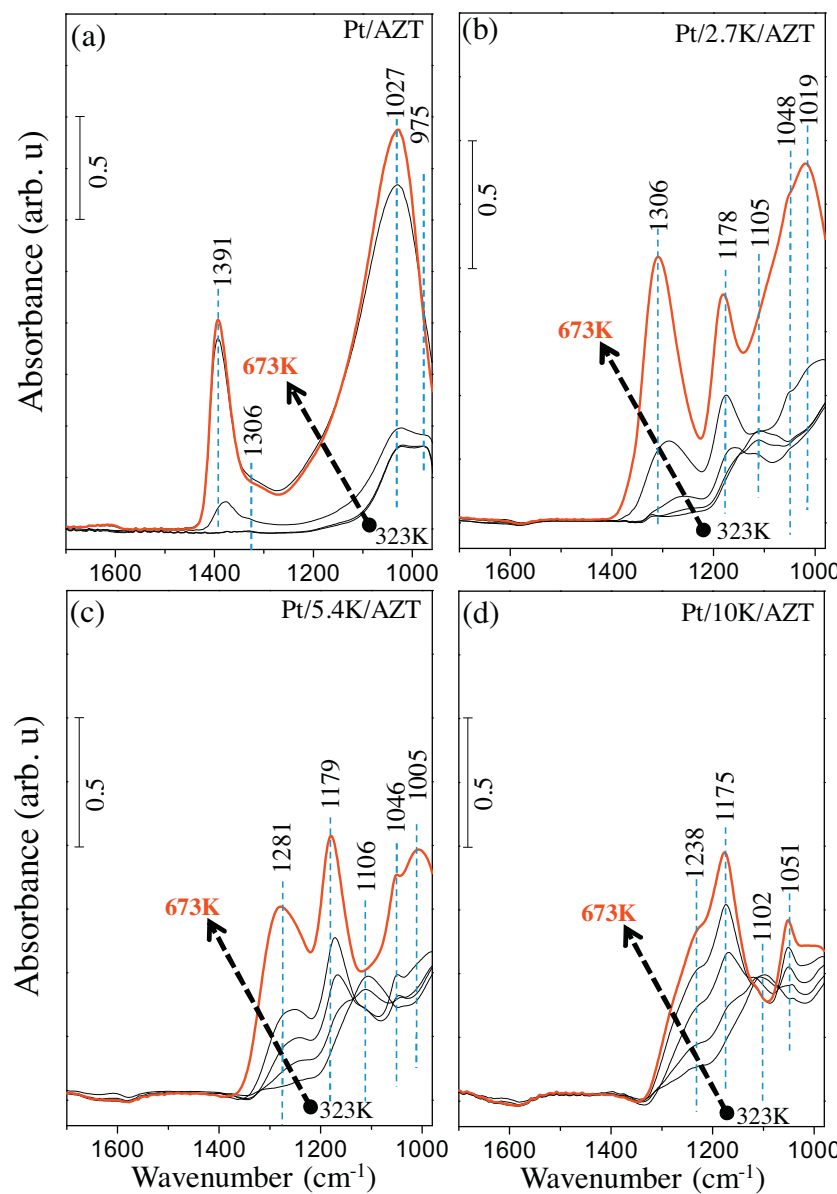


Fig. 3. FTIR spectra demonstrating the SO_x uptake/adsorption properties of (a) Pt/AZT, (b) Pt/2.7K/AZT(c) Pt/5.4K/AZT and (d) Pt/10K/AZT surfaces. Black set of spectra in each panel were acquired after SO_x exposure (2.0 Torr, $\text{SO}_2:\text{O}_2 = 1:10$) at 323 K, followed by annealing at 373, 473 and 573 K in the SO_x gas mixture for 15 min and subsequent evacuation. Red spectra in each panel were recorded after SO_x exposure at 673 K and subsequent evacuation. All spectra were recorded at 323 K in vacuum. (For the interpretation of the references to colour in this figure, the reader is referred to the web version of this article.)

Kim et al. reported that an increase in K_2O loading from 2 wt. % to 30 wt. % led to a boost in NSC of $\text{Pt}/\text{K}_2\text{O}/\text{Al}_2\text{O}_3$ materials within 600–800 K [34]. As will be demonstrated latter, although such extremely high K_2O loadings could be beneficial to enhance NSC in the absence of SO_x , they may also lead to irreversible sulfur poisoning in the presence of SO_x . Therefore, in the current study, we limited the K_2O loading of the AZT-based NSR/LNT materials to 10 wt. %.

Fig. 3a shows that SO_x adsorption on Pt/AZT at relatively lower temperatures (i.e. 323 and 373 K) leads to two main vibrational features located at 1027 and 975 cm^{-1} which can be assigned to sulfate (SO_4^{2-}) and sulfite (SO_3^{2-}) functional groups, respectively [35–39]. Absorbance intensities of these two particular vibrational frequencies are comparable at low temperatures, while the sulfate feature starts to dominate the sulfite feature at higher temperatures. Thermally-triggered catalytic oxidation of sulfite species to sulfates on the Pt/AZT surface can also be followed in Fig. 3a

by monitoring the growth of the antisymmetric stretching mode of surface sulfate groups located at 1391 and 1306 cm^{-1} [14,40]. As illustrated in Fig. 3b–d, addition of basic K_2O domains onto AZT ternary oxide system results in alteration of the spectral line shapes. Pt/2.7 K/AZT (Fig. 3b) presents five major vibrational features located at 1306, 1178, 1105, 1048 and 1019 cm^{-1} . While IR stretchings at 1306, 1105, 1048 and 1019 cm^{-1} can be attributed to the surface sulfate (SO_4^{2-}) groups on K_2O and/or on the AZT support, vibrational feature located at 1178 cm^{-1} can be attributed to bulk-like sulfate groups on K_2O [41,42]. This latter feature becomes more discernible with an increase in the K_2O loading (i.e. 5.4 wt. % and 10 wt. %) evident by the increasing relative absorbance intensity of the 1178 cm^{-1} signal in Fig. 3c and d. SO_x adsorption on Pt/5.4K/AZT and Pt/10K/AZT materials at 673 K leads to vibrational features at 1281 and 1238 cm^{-1} along with the absence of any significant vibrational bands located at ca. $> 1300 \text{ cm}^{-1}$ (Fig. 3c and d). The vibrational signals at 1281 and 1238 cm^{-1} can be assigned

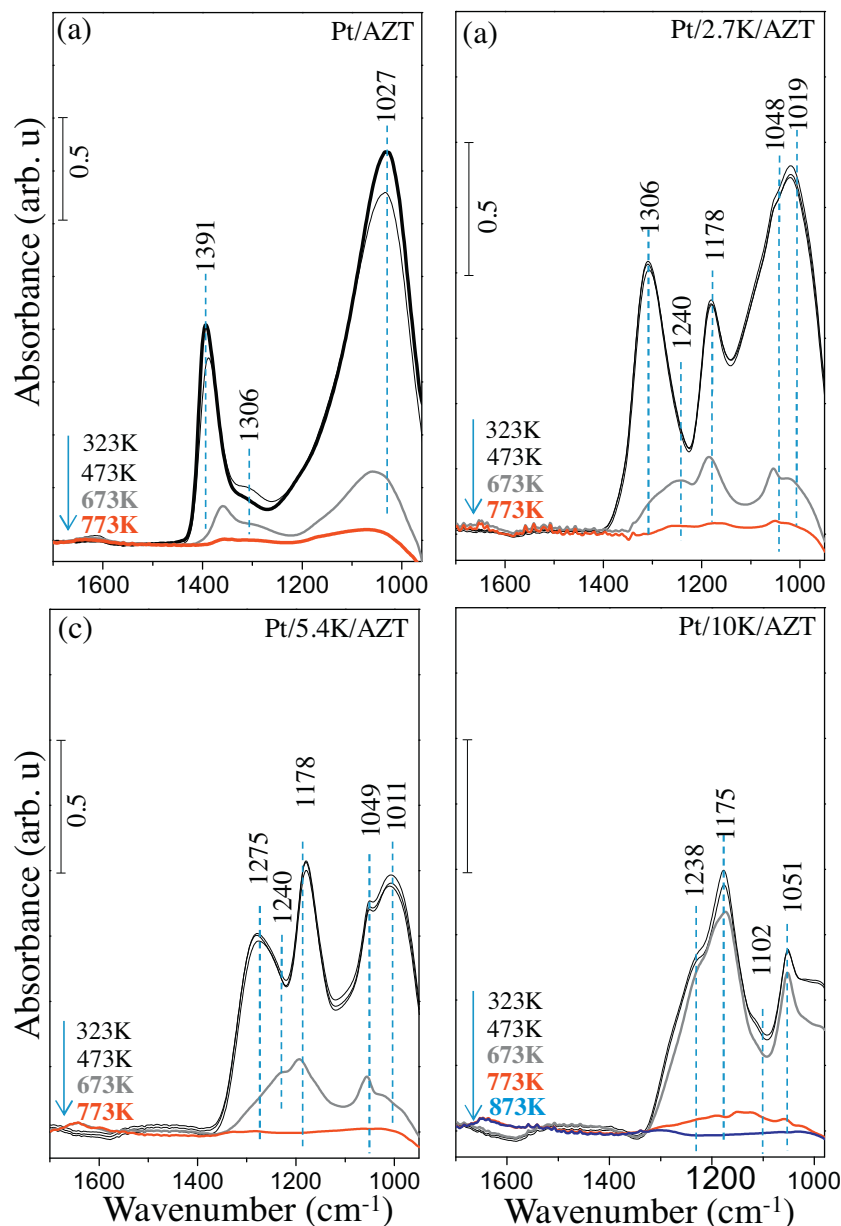


Fig. 4. FTIR spectra associated with SO_x reduction and regeneration of (a) Pt/AZT, (b) Pt/2.7K/AZT(c) Pt/5.4K/AZT and (d) Pt/10K/AZT materials via $\text{H}_2(\text{g})$. Catalysts were initially sulfated (2.0 Torr, $\text{SO}_2:\text{O}_2 = 1:10$ for 15 min at 673 K) followed by evacuation and subsequent exposure to $\text{H}_2(\text{g})$ (15.0 Torr) at 323, 473, 673, 773, 873 and 973 K for 5 min. All spectra were recorded at 323 K.

to predominantly sulfates on K_2O domains [14,41–43]. It can be argued that with the increasing K_2O loading, an increasingly larger portion of the AZT surface is covered by K_2O islands/domains, decreasing the extent of exposed/uncovered AZT surface. It is also likely that the increase in the K_2O loading also results in the growth of the K_2O particle size and formation of 3D agglomerates, enabling the storage of SO_x in the form of bulk-like sulfates in the sub-surface of these 3D nanoparticles. This argument is also in good agreement with the measured SSA values presented in Fig. 2 suggesting that the increase in the K_2O loading in the catalyst formulation leads to a monotonic decrease in the SSA as expected by sintering of the K_2O domains and particle size growth.

3.3. Sulfur regeneration with $\text{H}_2(\text{g})$ via in-situ FTIR spectroscopy

As mentioned above, SO_x reduction/regeneration performance has a significant influence on the catalyst lifetime and NO_x storage

capacity. Therefore, SO_x reduction characteristics of synthesized materials were also studied as a function of temperature by means of *in-situ* FTIR spectroscopy. Fig. 4 illustrates the evolution of the S-containing surface functional groups on Pt/AZT, Pt/2.7K/AZT, Pt/5.4K/AZT and Pt/10K/AZT catalyst surfaces as a function of temperature within 323–773 K in the presence of an external reducing agent, $\text{H}_2(\text{g})$.

In these set of experiments, catalysts were initially saturated with a 2.0 Torr of $\text{SO}_2 + \text{O}_2$ gas mixture ($\text{SO}_2:\text{O}_2 = 1:10$) at 673 K for 5 min and then cooled to 323 K followed by the evacuation of the spectroscopic reactor, introduction of 15.0 Torr $\text{H}_2(\text{g})$ at 323 K and annealing in $\text{H}_2(\text{g})$ at the given temperatures within 323–773 K. This particularly chosen initial sulfation/poisoning temperature (i.e. 673 K) is not only relevant to realistic NSR/LNT operational temperatures, but is also high enough to activate SO_2 oxidation to sulfites and sulfates in a comprehensive manner. In the series of experiments given in Fig. 4, spectral line shapes do not typi-

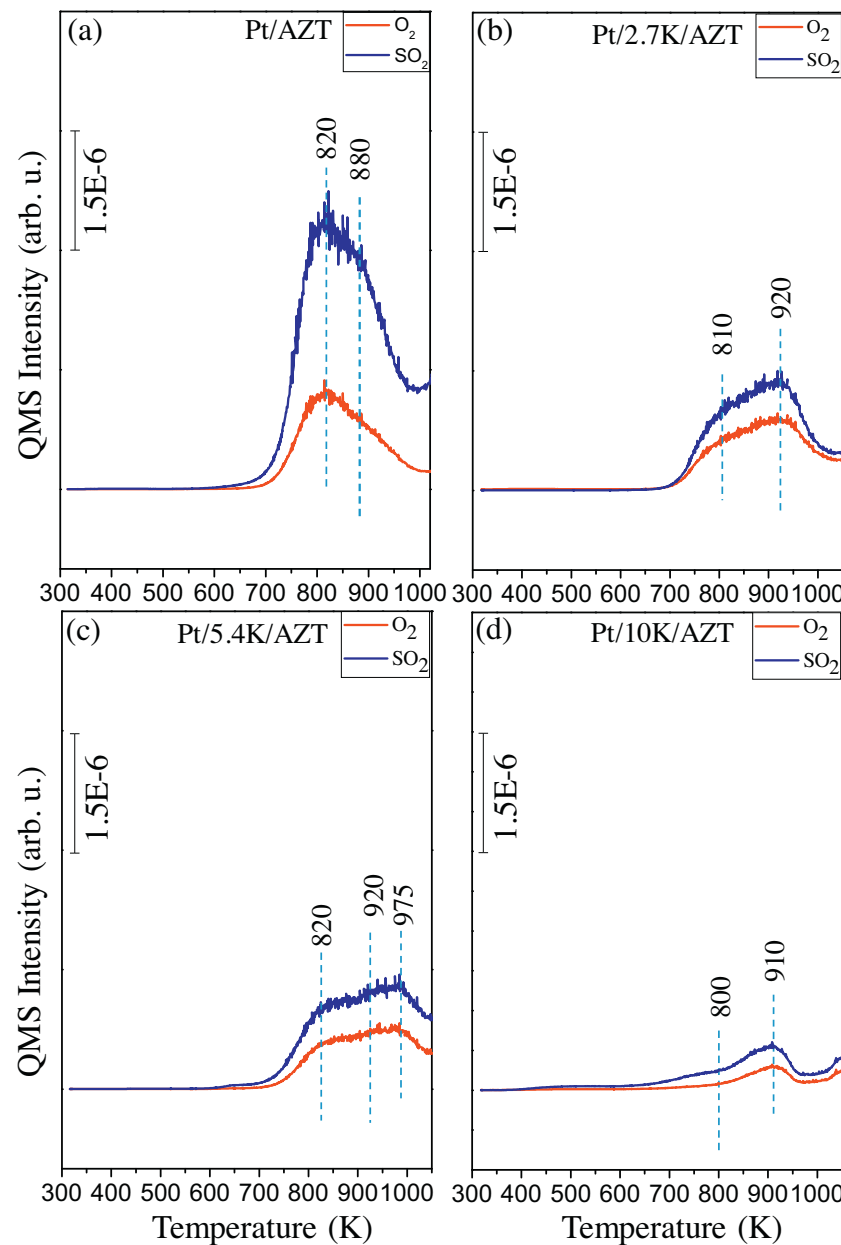


Fig. 5. TPD profiles for (a) Pt/AZT, (b) Pt/2.7K/AZT, (c) Pt/5.4K/AZT and (d) Pt/10K/AZT catalysts after 2.0 Torr SO_x (2.0 Torr SO₂ + O₂, SO₂:O₂ = 1:10) adsorption at 673 K for 30 min and subsequent evacuation.

cally change in a noteworthy manner at reduction temperatures ≤ 473 K. However, increasing the reduction temperature to 673 K (gray spectra in Fig. 4a–c) leads to noticeable alterations in the FTIR spectra, where bulk and surface sulfate/sulfite species significantly attenuate for Pt/AZT, Pt/2.7K/AZT and Pt/5.4K/AZT. Increasing the temperature to 773 K in the presence of H₂ leads to the almost complete elimination of the SO_x-related vibrational signatures on Pt/AZT, Pt/2.7K/AZT and Pt/5.4K/AZT surfaces (red spectra in Fig. 4a–c). It can be seen in Supporting information Fig. 1 that when Pt/20Ba/Al benchmark NSR/LNT catalyst is exposed to an identical set of sulfation and subsequent reduction treatments, a significantly greater portion of sulfate/sulfite species continue to exist on the Pt/20Ba/Al catalyst even at 773 K in the presence of 15.0 Torr H₂(g). This comparative analysis clearly suggests that Pt/AZT, Pt/2.7K/AZT and Pt/5.4K/AZT catalysts exhibit a superior sulfur regeneration performance than that of the Pt/20Ba/Al cata-

lyst, as this former set of materials can be fully de-sulfated at 773 K in the presence of H₂.

However, AZT-based catalysts with the highest K₂O loading used in the current study (*i.e.* Pt/10K/AZT) not only showed unique sulfur uptake characteristics as presented in Fig. 3d which is dominated by bulk-like sulfates, but also revealed a fairly different SO_x-reduction profile in the presence of H₂ (Fig. 4d). As can be seen in Fig. 4, at relatively low temperatures (*i.e.* T \leq 673 K), a significant portion of the SO_x species can already be eliminated from Pt/AZT, Pt/2.7K/AZT and Pt/5.4K/AZT surfaces. However, at T \leq 673 K, almost all of the S-related surface functional groups remain intact on Pt/10K/AZT. Even at a reduction temperature of 773 K, although Pt/AZT, Pt/2.7K/AZT surfaces can be fully regenerated (Fig. 4a–c), Pt/10K/AZT surface still remains partially blocked/poisoned by sulfur-containing functional groups and completely eliminated at only at ≥ 873 K (Fig. 4d).

3.4. Sulfur regeneration under vacuum via TPD analysis

TPD experiments were also carried out in vacuum in order to investigate the thermal regeneration ability of the synthesized catalysts after sulfur poisoning in the absence of a reducing agent, as well as to compare the relative adsorption strengths of SO_x species residing on the poisoned catalyst surfaces. Prior to TPD experiments, each catalyst was exposed to 2.0 Torr SO₂ + O₂ gas mixture (SO₂:O₂ = 1:10) at 673 K for 30 min.

Fig. 5 shows the TPD spectra corresponding to the thermal decomposition of sulfates and sulfites on Pt/AZT, Pt/2.7K/AZT, Pt/5.4K/AZT and Pt/10K/AZT catalyst surfaces. In these TPD experiments, only O₂ and SO₂ desorption channels (corresponding to mass to charge ratios of *m/z* = 32 and 64; respectively) revealed significant signals and other SO_x or H₂S species were not detectable. As in the case of the BaO-based conventional NSR/LNT catalyst (Supporting information Fig. 2), SO_x-related species adsorbed on Pt/AZT and its K₂O-incorporated counterparts reveal high thermal stability which is evident by the appearance of SO_x desorption signals at *T* > 700 K. Analysis of the general TPD line shapes given in Fig. 5a–c suggests that at least two different SO_x desorption signals exist for Pt/AZT, Pt/2.7K/AZT and Pt/5.4K/AZT catalysts at *T* < 1050 K, revealing desorption maxima located at *ca.* 800–820 K and at 900–975 K. Furthermore, SO₂ desorption on these surfaces within 700–1050 K is accompanied by O₂ desorption, suggesting that sulfate/sulfite decomposition occurs in the form of simultaneous SO₂ + O₂ release. It should be noted that the contribution of the SO₂ gas to the *m/z* = 32 signal due to electron-impact induced fragmentation of SO₂ in the QMS ionizer chamber is less than 10 %, suggesting that *m/z* = 32 signal can be almost exclusively attributed to the evolution of O₂(g) from the catalyst surfaces.

It is visible in Fig. 5a–c that the TPD desorption maxima tend to shift towards higher temperatures with increasing K₂O loading in the catalyst formulation. It can also be noticed that with increasing K₂O loading to 5.4 wt. % (see Fig. 5c), relative intensity of the 820 K desorption feature which can be mostly associated with SO_x species on AZT surface is suppressed, along with the generation of a high-temperature desorption shoulder at 975 K. This is in perfect agreement with the *in-situ* FTIR results presented in Fig. 3 suggesting that with increasing K₂O surface coverage, extent of exposed (uncovered) AZT surface decreases along with an increase in the K₂O particle size, facilitating the formation of bulk-like sulfates that are also thermally more stable than that of the sulfates on AZT.

It is also important to note that the SO_x desorption is not complete in Fig. 5b–d even at 1050 K (*i.e.* the highest experimentally attainable temperature in the current TPD setup) as evident by the presence of a desorption tail at *T* = 1050 K which is presumably extending well-beyond this temperature (as supported by the *in-situ* FTIR results that will be provided later in the text). This observation implies that while surface sulfates/sulfites present on AZT support and K₂O domains fully decompose at temperatures below 920 K, bulk-like potassium sulfate species require higher desorption temperatures for complete thermal decomposition and desorption. In other words, presence of basic K₂O domains yields strong binding sites for SO₂, leading to the formation of thermally stable surface and bulk-like SO_x species.

On the other hand, a further increase in the K₂O loading to 10 wt.% illustrates rather different SO_x desorption characteristics (Fig. 5d). It is evident that the SO_x desorption features at *T* < 1050 K are suppressed to a great extent, leading to a relatively minor desorption feature located at 910 K with a shoulder at *ca.* 810 K. Considering the significant SO_x uptake of the Pt/10K/AZT catalyst surface demonstrated by the *in-situ* FTIR data given in Fig. 3d, it is clear that most of the sulfate/sulfite species on Pt/10K/AZT remain intact even after vacuum annealing up to 1050 K. This is also quantitatively presented in Fig. 6, which presents the integrated SO₂ TPD

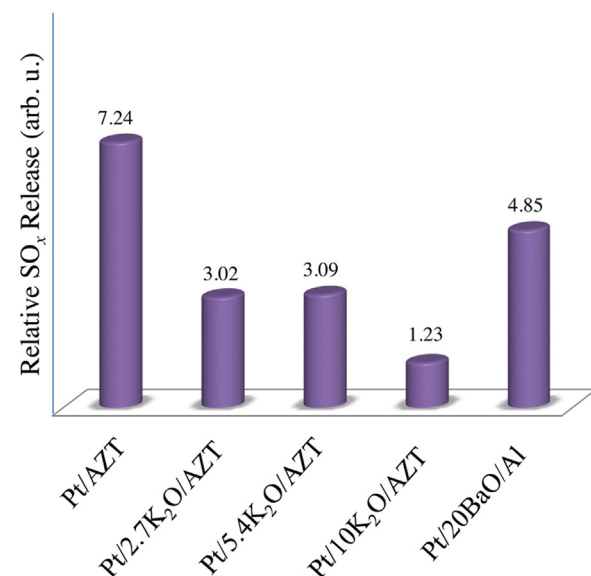


Fig. 6. Analysis of relative SO_x release from investigated catalysts calculated via integrated TPD signals given in Fig. 5.

desorption signals for the investigated AZT-based catalysts within 323–1050 K. Fig. 6 illustrates that the integrated SO_x desorption signal of Pt/AZT is roughly twice greater than that of Pt/2.7K/AZT and Pt/5.4K/AZT and also about four times greater than that of Pt/10K/AZT.

Figs. 3, 5 and 6, suggest that after the sulfation of the AZT-based catalysts at 673 K and a subsequent vacuum annealing up to 1050 K during the TPD experiments, a significant fraction of the sulfate and sulfite species remain intact on the K-containing sample surfaces. Thus, it is crucial to investigate the residual SO_x species remaining on the K-containing AZT systems after the TPD runs. Fig. 7 shows such *in-situ* FTIR experiments corresponding to all of the investigated sulfur poisoned AZT-based catalysts before (black spectra) and after (red spectra) TPD experiments. Fig. 7a clearly indicates that in the absence of K₂O, sulfur-poisoned Pt/AZT catalyst can be almost fully regenerated via vacuum annealing up to 1050 K during the TPD experiments. On the other hand, Pt/2.7K/AZT catalyst which releases about % 50 lesser amount of SO_x species during TPD (Fig. 6), still reveals a minor, yet readily detectable quantity of SO_x (Fig. 7b). On the other hand, Pt/5.4K/AZT catalyst which has a comparable integrated SO_x desorption signal to that of Pt/2.7K/AZT (Fig. 6), reveals a stronger residual SO_x signal in the FTIR spectrum obtained after the TPD run given in Fig. 7c. This observation is in line with the fact that Pt/5.4K/AZT surface stores a significantly greater amount of SO_x species (which are also thermally more stable) as compared to that of Pt/2.7K/AZT. Finally, residual sulfur analysis of the Pt/10K/AZT surface (Fig. 7d) indicates that almost all of the SO_x species generated during initial poisoning process remain intact after the TPD run and vacuum annealing at 1050 K. Thus, it is apparent that the minor amount of SO_x release during the TPD experiment for Pt/10K/AZT (Fig. 6) corresponds to a tiny fraction of the overall sulfur that is stored on this surface. This latter result has some resemblance to the TPD data corresponding to that of the Pt/20Ba/Al benchmark catalyst given in Supporting information Figs. 2 and 3 and also in Fig. 6 which also reveal an incomplete thermal regeneration upon vacuum annealing up to 1050 K during the TPD run.

We also performed a comprehensive investigation of the NO_x storage, release and reduction characteristics of Pt/K/AZT systems via *in-situ* FTIR, TPD as well as quantitative flow-reactor experiments [44]. A detailed account of these additional experiments will

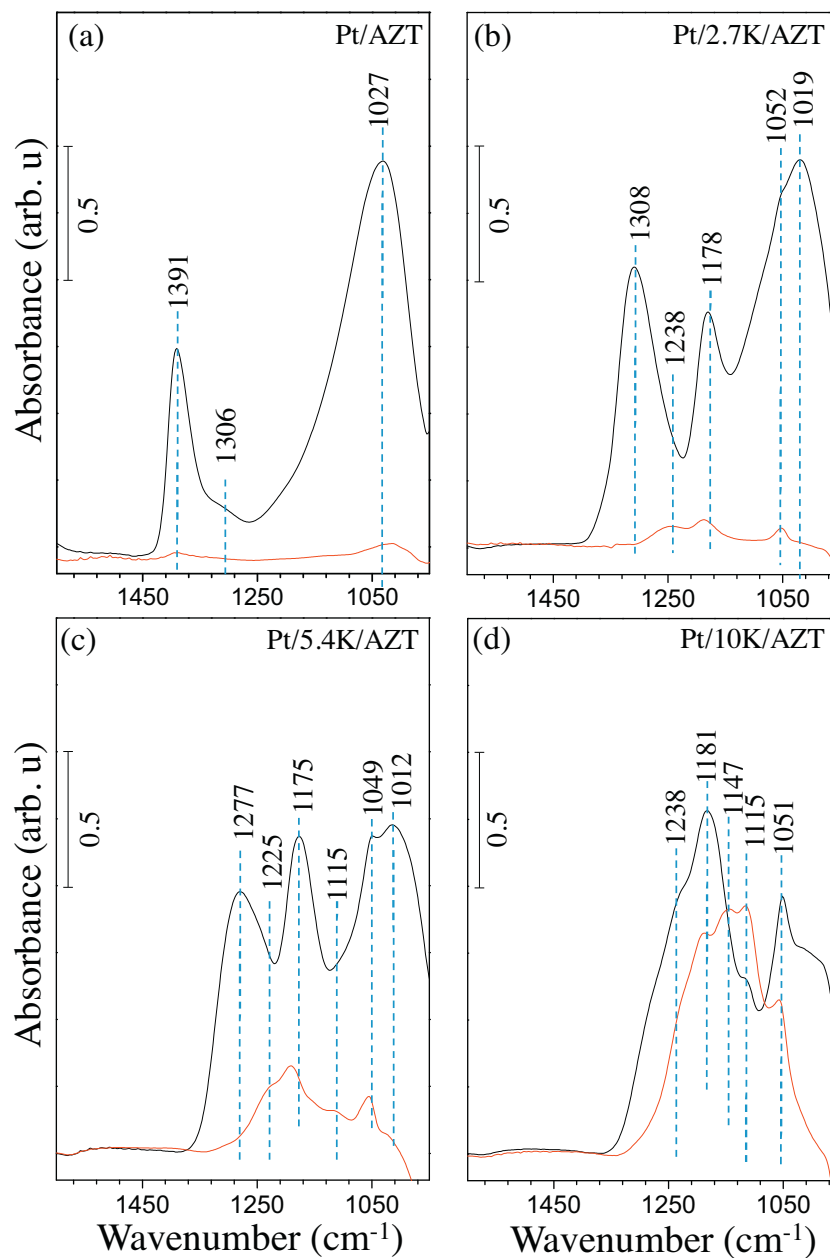


Fig. 7. FTIR spectra corresponding to SO_x content of (a) Pt/AZT, (b) Pt/2.7K/AZT, (c) Pt/5.4K/AZT and (d) Pt/10K/AZT catalysts before (black) and after (red) SO_x-TPD runs. (For interpretation of the references to colour in this figure legend, the reader is referred to the web version of this article.)

be discussed thoroughly in a forthcoming report. Nevertheless, it is instructive to present relative integrated TPD NO_x desorption signals obtained after saturation of the freshly prepared AZT-based catalysts with NO₂ (5.0 Torr NO₂ at 323 K for 10 min) in the absence of sulfur as compared to that of the Pt/20Ba/Al benchmark catalyst (Fig. 8). As can be seen in Fig. 8, relative NO_x storage amounts of the AZT-based catalysts increase monotonically with increasing K₂O loading until 5.4 wt. % K₂O, after which it converges to a value that is comparable to that of the Pt/20Ba/Al benchmark catalyst. It is worth mentioning that NSC of the synthesized materials were investigated in a flow-mode tubular reactor where the inlet gas feed was composed of 500 ppm NO, v.% 5 O₂, v.% 5 CO₂ and v.% 5 H₂O balanced with Ar(g), revealing similar NSC values for Pt/5.4K/AZT (0.165 mmol/g_{cat}) and conventional Pt/20Ba/Al (0.171 mmol/g_{cat}) at 573 K [44].

A combined analysis of the structural characterization results as well as the spectroscopic probe molecule adsorption experiments given in the current study allows us to shed light on sulfur poisoning, regeneration and NO_x storage characteristics of AZT-based NSR/LNT catalysts functionalized with K₂O. In the absence of the K₂O, Pt/AZT system reveals high SSA (191 m²/g) and relatively weakly bound sulfates/sulfites which can readily be removed from the surface in a complete fashion either by reduction with H₂(g) at 773 K or simply by thermal regeneration in vacuum at ca. 950 K. However, due to lack of basic K₂O domains, Pt/AZT suffers from relatively low NSC. Increasing the K₂O loading to 2.7, 5.4 and 10.0 wt.% leads to a progressively increasing NO_x adsorption where NSC seems to be converging to a value similar to that of Pt/20Ba/Al benchmark catalyst for Pt/5.4K/AZT and Pt/10K/AZT. Furthermore, Pt/5.4K/AZT sample allows complete removal of SO_x via H₂(g) at 773 K unlike the conventional Pt/20Ba/Al benchmark

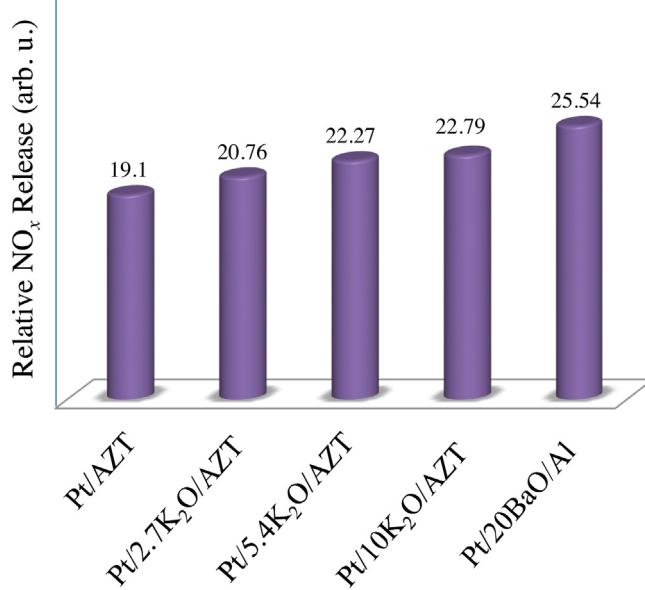


Fig. 8. Relative integrated NO_x desorption signals obtained from NO_x-TPD experiments.

catalyst whose complete regeneration requires much higher temperatures (*i.e.* 973 K) under identical reducing conditions. Although increasing the K₂O loading from 5.4 to 10.0 wt. % does not seem to have a tremendous enhancement in NO_x adsorption properties of the Pt/K/AZT system, it does result in unfavorable SO_x uptake, release and regeneration characteristics. TPD and FTIR data suggest that K₂O domains tend to agglomerate with increasing K₂O loading and form 3D clusters with growing K₂O particle sizes. These phenomena also expedite the formation of bulk-like sulfate functionalities in the subsurface of K₂O domains with much higher thermal stability and much stronger resistance against thermal decomposition and reduction with hydrogen. Consequently, Pt/5.4K/AZT system appears as a promising alternative which can also be used in conjunction with conventional Pt/20Ba/Al NSR/LNT catalysts.

4. Conclusion

In the current study, advanced ternary and quaternary mixed oxide materials in the form of Pt/K₂O/Al₂O₃/ZrO₂/TiO₂ were synthesized with different K₂O loadings. Synthesized materials were structurally characterized *via* XRD and BET in comparison to a conventional Pt/20Ba/Al benchmark NSR/LNT catalyst. Interaction of these catalyst surfaces with SO_x (*i.e.* SO₂ + O₂) mixture were monitored spectroscopically using *in-situ* FTIR and TPD. Our findings can be summarized as follows:

- Besides the presence of ordered metallic Pt, Pt/AZT, Pt/2.7K/AZT and Pt/5.4K/AZT materials revealed disordered structures. On the other hand, Pt/10K/AZT exhibited additional diffraction signals corresponding to tetragonal ZrO₂ domains. Unlike the AZT-supported materials, conventional Pt/20Ba/Al benchmark catalyst was composed of ordered phases including γ-Al₂O₃ and BaAl₂O₄.
- Increase in K₂O loading from 2.7 to 5.4 and 10.0 wt. % monotonically decreases the SSA values from 177 m²/g to 155 and 125 m²/g, respectively. Apart from the Pt/10K/AZT catalyst, SSA values of the corresponding Pt/K/AZT catalysts are higher than that of the benchmark Pt/20Ba/Al catalyst (134 m²/g).

- Increasing the K₂O loading in the Pt/K/AZT system leads to the growth of the K₂O domain size (*i.e.* sintering), covering of the AZT surface with K₂O and an increase in the bulk-like sulfate functional groups requiring higher temperatures for complete sulfur elimination *via* thermal decomposition or *via* reduction with H₂(g).
- Increase in K₂O loading in the Pt/K/AZT formulation increases the NO_x adsorption up to 5.4 wt. % of K₂O. However K₂O loadings higher than this value do not have a significant positive influence on NO_x adsorption.
- There is a delicate trade-off between NSC and sulfur adsorption/release/regeneration characteristics. NSC and SO_x tolerance of AZT based NSR/LNT catalysts can be optimized simultaneously by carefully fine-tuning the K₂O loading.
- Among the investigated catalysts, Pt/5.4K/AZT was found to reveal superior sulfur regeneration performance than that of the conventional Pt/20Ba/Al benchmark catalyst along with a comparable NSC (0.165 vs. 0.171 mmol/g_{cat}, respectively).

Acknowledgements

Authors acknowledge the financial support from the Scientific and Technological Research Council of Turkey (TUBITAK) (Project Code: 111M780). Authors also acknowledge Prof. Louise Olsson and Oana Mihai (Chalmers University of Technology) for quantitative flow-mode NSC measurements.

Appendix A. Supplementary data

Supplementary data associated with this article can be found, in the online version, at <http://dx.doi.org/10.1016/j.cattod.2015.12.013>.

References

- [1] F. Klingstedt, K. Arve, K. Eränen, D.Y. Murzin, *Acc. Chem. Res.* 39 (2006) 273–282.
- [2] W.S. Epling, L.E. Campbell, A. Yezerets, N.W. Currier, J.E. Parks, *Catal. Rev. Eng.* 46 (2004) 163–245.
- [3] S. Matsumoto, *CATTECH* 4 (2000) 102–109.
- [4] A. Fritz, V. Pitchon, *Appl. Catal. B Environ.* 13 (1997) 1–25.
- [5] Q. Schiermeier, The science behind the Volkswagen emissions scandal, in: *Nat. News*, 2015.
- [6] <<http://www.eea.europa.eu/publications/nec-directive-status-report-2014>>.
- [7] K. Kato, H. Nohira, K. Nakanishi, S. Iguchi, T. Kihara, H. Muraki, Euro Patent application 0,573,672 A1, 1993.
- [8] N. Myoshii, S. Matsumoto, K. Katoh, T. Tanaka, K. Harada, N. Takahashi, K. Yokota, M. Sugiyura, K. Kasahara, SAE Technical Papers Series No. 950809, 1995.
- [9] S. Roy, A. Bajer, *Chem. Rev.* 109 (2009) 4054–4091.
- [10] Z. Say, E.I. Vovk, V.I. Bukhtiyarov, E. Ozensoy, *Appl. Catal. B Environ.* 142–143 (2013) 89–100.
- [11] W.S. Epling, D. Kisinger, C. Everest, *Catal. Today* 136 (2008) 156–163.
- [12] D.H. Kim, Y. Chin, G.G. Muntean, A. Yezerets, N.W. Currier, W.S. Epling, H. Chen, H. Hess, C.H.F. Peden, *Ind. Eng. Chem. Res.* 45 (2006) 8815–8821.
- [13] S.M. Andonova, G.S. Şentürk, E. Kayhan, E. Ozensoy, *J. Phys. Chem. C* 113 (2009) 11026.
- [14] Z. Say, E.I. Vovk, V.I. Bukhtiyarov, E. Ozensoy, *Top. Catal.* 56 (2013) 950–957.
- [15] T. Szailer, J.H. Kwak, D.H. Kim, J.C. Hanson, C.H.F. Peden, J. Szanyi, *J. Catal.* 239 (2006) 51–64.
- [16] I.S. Pieta, M. García-Díéguez, C. Herrera, M. a. Larrubia, L.J. Alemany, *J. Catal.* 270 (2010) 256–267.
- [17] K.S. Kabin, P. Khanna, R.L. Muncrief, V. Medhekar, M.P. Harold, *Catal. Today* 114 (2006) 72–85.
- [18] S. Morandi, F. Pinetto, G. Ghiootti, L. Castoldi, L. Lietti, P. Forzatti, M. Daturi, V. Blasin-Aubé, *Catal. Today* 231 (2014) 116–124.
- [19] D.H. Kim, K. Mudiyanselage, J. Szanyi, H. Zhu, J.H. Kwak, C.H.F. Peden, *Catal. Today* 184 (2012) 2–7.
- [20] M. Takeuchi, S. Matsumoto, *Top. Catal.* 28 (2004) 151–156.
- [21] T.J. Toops, D.B. Smith, W.P. Partridge, *Catal. Today* 114 (2006) 112–124.
- [22] J. Luo, F. Gao, D.H. Kim, C.H.F. Peden, *Catal. Today* 231 (2014) 164–172.
- [23] E. Fridell, H. Persson, L. Olsson, B. Westerberg, A. Ambergsson, M. Skoglundh, *Top. Catal.* 16/17 (2001) 133.
- [24] J. Escobar, J.A. De los Reyes, T. Viveros, *Ind. Eng. Chem. Res.* 39 (2000) 666.
- [25] Z. Say, M. Tohumeken, E. Ozensoy, *Catal. Today* 231 (2014) 135.

- [26] M. Meng, L. Guo, J. He, Y. Lai, Z. Li, X. Li, *Catal. Today* 175 (2011) 72.
- [27] Z.Q. Zou, M. Meng, X.Y. Zhou, X.G. Li, Y.Q. Zha, *Catal. Lett.* 128 (2009) 475.
- [28] N. Takahashi, A. Suda, I. Hachisuka, M. Sugiura, H. Sobukawa, H. Shinjoh, *Appl. Catal. B Environ.* 72 (2007) 187.
- [29] H. Imagawa, T. Tanaka, N. Takahashi, S. Matsunaga, A. Suda, H. Shinjoh, *J. Catal.* 251 (2007) 315.
- [30] H. Imagawa, N. Takahashi, T. Tanaka, S. Matsunaga, H. Shinjoh, *Appl. Catal. B Environ.* 92 (2009) 23.
- [31] Z.Q. Zou, M. Meng, J. He, *Mater. Chem. Phys.* 124 (2010) 987.
- [32] Z. Say, M. Dogac, E.I. Vovk, Y.E. Kalay, C.H. Kim, W. Li, E. Ozensoy, *Appl. Catal. B Environ.* 154–155 (2014) 51.
- [33] L.E. Venegas, N.A. Mazzeo, A.L.P. Rojas, *Air Qual. Appl., In Tech.*, 2011, ISBN: 978-953-307-307-1.
- [34] D.H. Kim, K. Mudiyanselage, J. Szanyi, J.H. Kwak, H. Zhu, C.H.F. Peden, *Appl. Catal. B Environ.* 142–143 (2013) 472–478.
- [35] M. Kantcheva, E.Z. Ciftlikli, *J. Phys. Chem. B* 106 (2002) 3941–3949.
- [36] C. Chang, *J. Catal.* 53 (1978) 374–385.
- [37] M. Waqif, *Solid State Ionics* 95 (1997) 163–167.
- [38] O. Saur, M. Bensitel, A.B. Mohammed Saad, J.C. Lavalle, C.P. Tripp, B.A. Morrow, *J. Catal.* 99 (1986) 104–110.
- [39] H. Yao, H.K. Stepien, H.S. Gandhi, *J. Catal.* 67 (1981) 231–236.
- [40] G.S. Şentürk, E.I. Vovk, V.I. Zaikovskii, Z. Say, A.M. Soylu, V.I. Bukhtiyarov, E. Ozensoy, *Catal.Today* 184 (2012) 54–71.
- [41] C. Sedlmair, K. Seshan, A. Jentys, J. Lercher, *Catal. Today* 75 (2002) 413–419.
- [42] Y. Liu, M. Meng, X.G. Li, L.H. Guo, Y.Q. Zha, *Chem. Eng. Res. Des.* 86 (2008) 932–940.
- [43] H. Abdulhamid, E. Fridell, J. Dawody, M. Skoglundh, *J. Catal.* 241 (2006) 200–210.
- [44] Z. Say, O. Mihai, M. Tohumeken, L. Olsson, E. Ozensoy, in preparation.